THE JOURNAL OF NAVIGATION (2003), **56**, 457–473. © The Royal Institute of Navigation
DOI: 10.1017/S0373463303002376 Printed in the United Kingdom

A Triple Difference Approach to Low Earth Orbiter Precision Orbit Determination

Jay Hyoun Kwon

(*Sejong University*, *Korea*)

Dorota Grejner-Brzezinska, Tae-Suk Bae and Chang-Ki Hong

(*Ohio State University*)

A geometric approach to Low Earth Orbiter (LEO) precision orbit determination (POD) based exclusively on triple-differenced GPS carrier phase observables is presented. The algorithm is fast and efficient because there is no ambiguity-resolution requirement, which is a complicated and time-consuming task for long-range kinematic GPS. However, the triple-difference kinematic LEO POD requires careful screening for cycle slips, as the orbit quality depends on the accuracy and the geometry of the observations. It is shown that the signal-to-noise-ratio (SNR) combined with residual screening offers a good approach to data cleaning. Data from a CHAMP (Challenging Minisatellite Payload, altitude $\sim$450 km) mission are used to present the accuracy, speed and efficiency of the processing algorithms. The methods of data screening and the effects of geometry on the orbit quality are discussed and the final achievable accuracy including the limitations and benefits of this method are quantified. It is demonstrated that the triple-difference method offers short processing times and is currently capable of achieving a 3D RMS fit to the dynamic orbit of 15–30 cm and 1 mm/s to the velocity.

KEY WORDS

1. Low Earth Orbiter. 2. GPS.

1. INTRODUCTION. This paper presents of the development and implementation of a fast, accurate and efficient technique for Low Earth Orbiter (LEO) trajectory estimation with a kinematic method based on triple-differenced GPS carrier phase observables. The triple-difference approach provides a very efficient kinematic precision orbit determination (POD) procedure, primarily due to the removal through time differencing of the integer ambiguity parameters. The triple-difference technique presented here was derived from the modified version of the GPS POD software, GODIVA, developed at the Ohio State University (Grejner-Brzezinska, (1995); Yang, (1995); Goad et al., (1996); Kwon, (1997)). After removing all dynamic force models used in GODIVA, the processing was changed to an efficient forward and backward batch estimator for kinematic LEO POD, named Precise Kinematic Orbit Determination software (P-KOD). The rationale for the

https://doi.org/10.1017/S0373463303002376 Published online by Cambridge University Press

kinematic approach to LEO orbit determination (OD) is the simplicity of the method, the short processing time, and the underlying fact that, particularly at lower altitudes, the actual trajectory may be closer to the precise GPS position rather than the trajectory determined by use of dynamic force models. On low earth orbits the complicated irregularly shaped spacecraft may be precisely positioned without using the sophisticated force models required for the dynamic method.

In spite of the obvious advantages of the kinematic OD approach, there are also some inherent problems related to the method's sensitivity to weak GPS/LEO/tracking station geometry. The orbit quality degrades and cannot be bridged by force modelling, as can be done in reduced dynamic or dynamic approaches. In GPS-based OD, especially with a geometric approach, the varying tracking station geometry and the station number along the LEO paths have a profound impact on the overall orbit accuracy. Since our ultimate objective is to provide quality orbits supporting atmospheric limb sounding in near real-time (limited virtually by the tracking data availability), it is important that the number and distribution of the selected subset of the IGS tracking stations provide continuous and reliable solutions. Even if the selected station coverage is sufficient, any data gaps in LEO will introduce a discontinuity in the kinematic trajectory. Another complication of the kinematic OD process is the need for a reliable procedure of cycle slip (CS) determination. This is a rather complicated process for a fast moving dynamic platform where the tracking geometry and the ionosphere both change rapidly over the commonly used data sampling rate (a 30-second rate is used here to demonstrate the method's performance).

This paper is a continuation of our previous work (Grejner-Brzezinska et al., (2001); Bae et al., (2002); Grejner-Brzezinska et al., (2002a and 2002b); Kwon et al., (2002)), where the initial implementation and preliminary performance analysis were presented. In this paper we discuss the final algorithmic implementation, including the modification of the data cleaning procedure, and the extended performance analysis. The kinematic approach to LEO OD has been addressed in the literature (for example, Byun, (1998); Byun and Schutz, (2002); Bisnath and Langley, (1999, 2001a and 2001b); Bock et al., (2001); Svehla and Rothacher, (2001 and 2002)). In this paper, we use the CHAMP satellite data to demonstrate the performance and the efficiency of the kinematic data processing algorithm, which can support atmospheric science missions in near-real time with sufficient accuracy.

1.1. *CHAMP mission: major objectives.* The German scientific satellite CHAMP (Challenging Minisatellite Payload; see, for example, Reigber et al., (2002); Koenig et al., (2002); http://op.gfz-potsdam.de/champ/index_CHAMP.html), was launched on July 15, 2000, into an almost circular, near polar ($I = 87^{\circ}$) orbit with an initial altitude of 454 km. Due to atmospheric drag, the altitude will decrease over the five-year mission lifetime. The primary science objectives of the mission are:

(1) To provide highly precise global long-wavelength features of the static Earth gravity field and the temporal variations of this field,
(2) To provide unprecedented accuracy global estimates of the main and crustal magnetic field of the Earth and the space/time variability of these field components, and
(3) To provide a good global distribution of a large number of GPS signal refraction data caused by the atmosphere and ionosphere at the event of satellite occultation by the Earth atmosphere, which can be converted into

https://doi.org/10.1017/S0373463303002376 Published online by Cambridge University Press

temperature, water vapour and electron content profiles (http://op.gfz-potsdam.de/champ/).

The atmospheric science objective mandates the availability of CHAMP orbits in near real time, to enable the use of the occultation data in numerical weather modelling and forecasting.

The TSRS-2 is the self-initializing and autonomous NASA BlackJack receiver assembly onboard CHAMP. It is a 16-channel receiver that can simultaneously track a maximum of 12 satellites for OD data collection with a sampling rate of 0·1 Hz. BlackJack has enhanced capabilities over the older generation instrument used for GPS/MET mission; these include enhanced codeless tracking, a higher SNR and lower tracking in the atmosphere. In the occultation mode the receiver can track up to four GPS satellites at a 50 Hz sampling rate. The measurement noise for the navigation mode is about 2 mm for the carrier phases and about 30 cm for the pseudoranges. The GPS antennas used on CHAMP are: a choke ring zenith-mounted antenna for OD, a spare OD antenna mounted on the aft panel, a high-gain helix antenna for occultation measurements mounted on the aft panel and a high-gain nadir-viewing helix antenna for GPS altimetry experiments (http://op.gfz-potsdam.de/champ/).

2. DATA PROCESSING ALGORITHM.

The earth-centered-earth-fixed (ECEF) coordinates of the tracking stations, the GPS tracking data from the stations and the LEO, and the GPS satellites trajectories are all required to carry out the LEO POD. Currently, the precise GPS orbits and well-distributed tracking station data provided by the International GPS Service (IGS) are utilized in our data processing routines. The ionospheric effect is removed by constructing triple-differenced ionosphere-free combinations and the Hopfield tropospheric model is used to account for the tropospheric delays. Thus, the only unknowns in the P-KOD solution are the epoch-by-epoch position coordinates of the LEO satellite. The P-KOD processing scheme consists of the three main procedures: (1) pre-processing of GPS data, (2) the main estimation of LEO POD, and (3) the post-processing of the estimated orbit, i.e., possible smoothing and velocity estimation, shown in Figure 1. In the pre-processing step the triple difference database is constructed, the receiver clock errors estimated, and the initial scanning for cycle slips is performed. In the main processing step the normal matrix is accumulated for a preselected batch length (or for batches separated by singularity points or data gaps), and the system is solved in the forward processing mode. If the initial coordinates at the starting epoch are not known with sufficient accuracy, backward processing is performed, leading to much better positioning accuracy, as shown in Table 1 (the reference solution is the dynamic orbit, Rapid Science Orbit (RSO) provided by GFZ). The forward/backward filtering can be repeated for increased accuracy. More details on the processing routines can be found in Grejner-Brzezinska et al., (2002a); Kwon et al., (2002).

2.1. *Cycle slip detection.*

Since the accuracy of the kinematic approach completely depends on the quality of measurements, cycle slips and outliers might significantly degrade the accuracy of the final orbit. Consequently, cycle slip detection is one of the most important components of the kinematic orbit determination process.

https://doi.org/10.1017/S0373463303002376 Published online by Cambridge University Press

Table 1. Fit (RMS) of the kinematic solution to RSO after forward and backward filtering, 500-epoch batch.

	RMS_x [m]	RMS_y [m]	RMS_z [m]	RMS_{3D} [m]
Forward	1·15	2·22	0·79	2·62
Backward	0·11	0·20	0·15	0·27

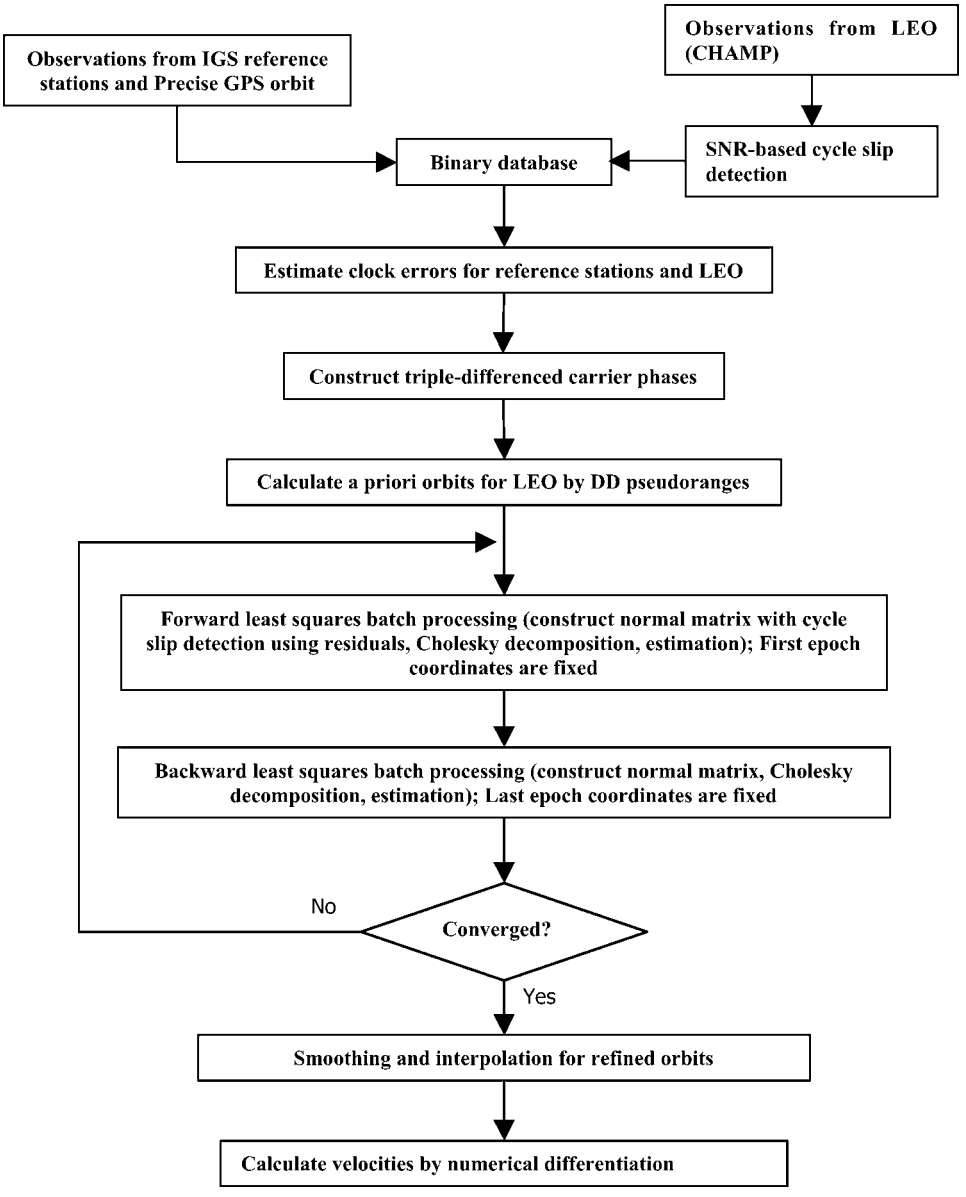


Figure 1. Schematic diagram of the kinematic LEO POD.

https://doi.org/10.1017/S0373463303002376 Published online by Cambridge University Press

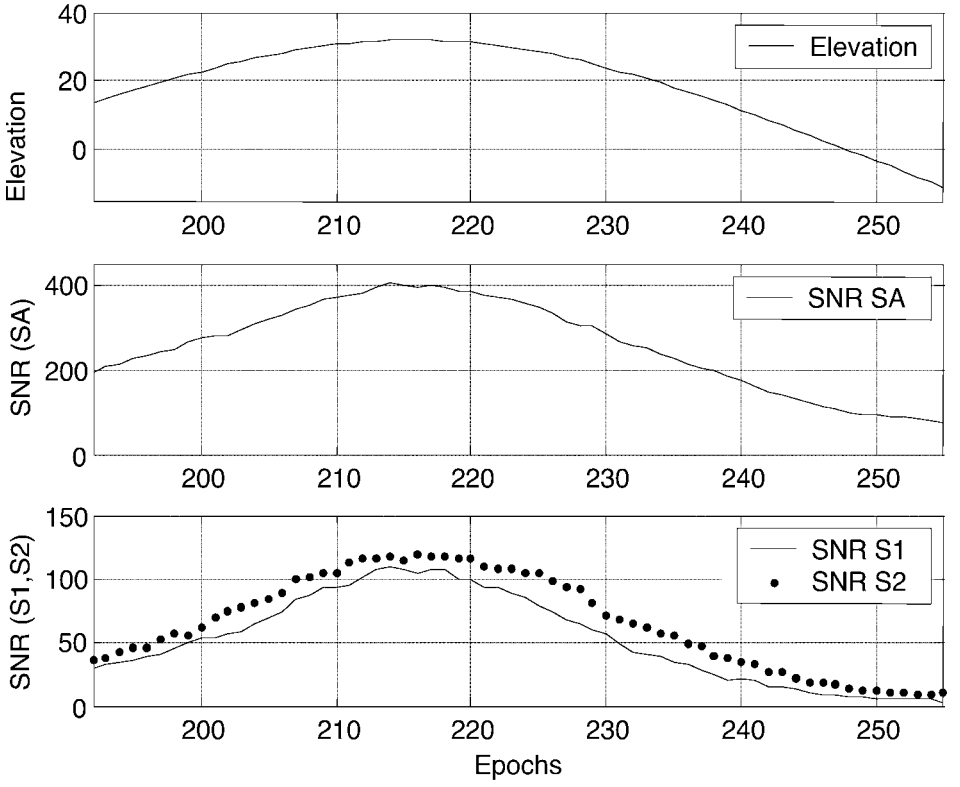


Figure 2. SNR values for CHAMP data.

One way to detect the cycle slips and outliers, assuming the availability of a good *a priori* orbit (must be better than the double-differenced kinematic pseudorange solution), is testing the least squares residuals against the predefined threshold. In general, the large residuals are treated as outliers (CS) and are removed from the data set. We do not attempt CS fixing, as in triple differencing CS affects only a single epoch, so the affected observables are simply discarded. If a good approximated orbit is not available, the cycle slips could be detected at the raw data level by investigating (1) ionosphere-only linear phase combination, and (2) phase/code combination, as well as (3) widelane ambiguity based on the double-difference phase-code combination. Our earlier approach, based on the above-mentioned techniques, is described in detail in Grejner-Brzezinska et al., (2002b) and Bae et al., (2002). Since this method does not always provide fully satisfactory results for CHAMP data, we extended our procedure to using SNR for CS detection, which can be followed by one of the data screening methods listed above. Three types of SNR are available for CHAMP data: S1 and S2 corresponding to L1 and L2 carrier phase channels, and SA, corresponding to the C/A channel. Figure 2 illustrates a typical behaviour of SNR for CHAMP data. Figure 3 illustrates the assessment of CS detection using SNR. The "true" reference is the number of CS detected by the analysis of triple-difference residuals using a dynamic orbit (RSO) with the cutoff of 20 cm. Figure 3 shows the total number of cycle slips detected by SNR and the number of CS detected by SNR that

https://doi.org/10.1017/S0373463303002376 Published online by Cambridge University Press

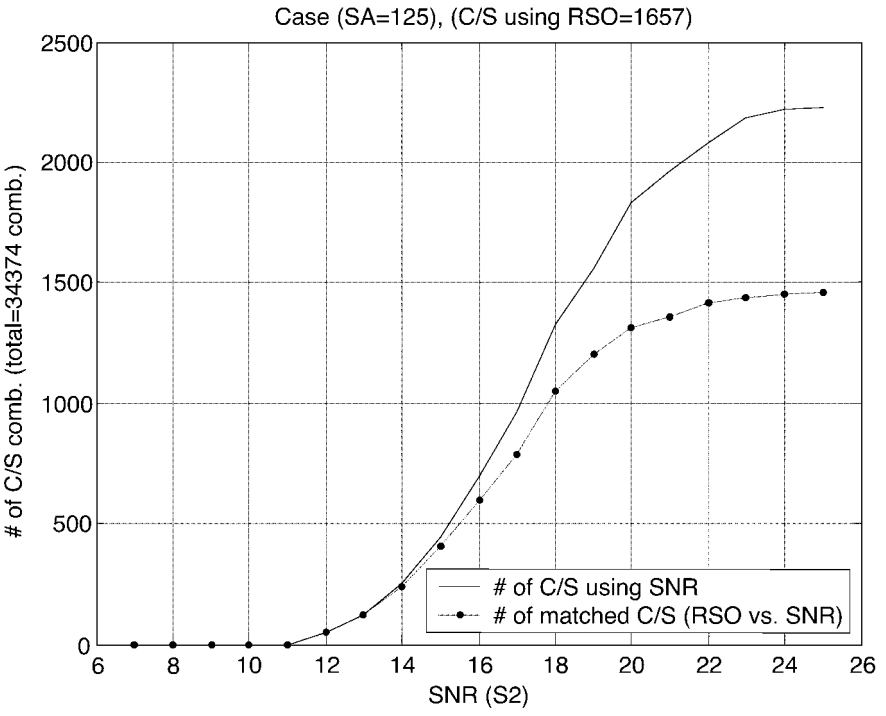


Figure 3. Comparison of cycle slips by SNR and RSO with fixed SA.

matched the reference method. The threshold level for SA was selected at 120, based on extensive prior testing, and several levels of S2 were tested. A total of 1657 CS were detected by testing the triple-difference residuals based on RSO, while the SNR method indicated a higher number of CS, depending on the selected SNR threshold level. It should be noted that finding the proper threshold of SA and S1 or S2 combination is not a trivial task. Moreover, the selected cutoff values for one day might not apply to another CHAMP data set. This variability of the SNR levels needs more attention.

Table 2 shows another example of different SNR combinations by varying SA with a fixed S2 threshold. The number of cycle slips matched between SNR-based and the reference solutions varies from 80 to 85 per cent, with SA ranging from 120 to 125. Effectively, if the RSO-based solution is considered "true reference," the SNR-based method might discard too many data points whilst leaving undetected a number of real CS. Based on the results presented in Table 2, it can be concluded that the number of detected cycle slips will vary depending on the SNR threshold selected, and will affect the accuracy of the estimated orbits. Based on the analysis presented in Table 2, a data set was cleaned and used for the orbit determination. This solution provided a less smooth orbit with a 3D-RMS fit to RSO of 33 cm. It is about a 22 per cent decrease in accuracy compared to the solution with cycle slips detected based on triple-difference residuals using a good *a priori* orbit (3D RMS = 27 cm). Consequently, the application of a smoother using either a 9th degree polynomial or a sliding 20-epoch wide window can clean the orbit from the remaining spikes due to undetected CS (see Section 4.2).

https://doi.org/10.1017/S0373463303002376 Published online by Cambridge University Press

Table 2. Comparison of cycle slips detected by SNR and RSO with fixed S2 (Grejner-Brzezinska et al., (2002a)).

SA	S2	Number of C/S	Number of matched C/S
120	22	1708 (5·0%)	1336 (80·6%)
121	22	1817 (5·3%)	1354 (81·7%)
122	22	1910 (5·7%)	1372 (82·8%)
123	22	1938 (5·6%)	1395 (84·2%)
124	22	1984 (5·8%)	1415 (85·4%)
125	22	2099 (6·1%)	1417 (85·5%)

2.2. *Ion-free triple-difference carrier phase observations.* Using the dependency of the ionospheric effect on the frequency, an ionosphere-free measurement can be obtained by combining the phase observations as follows:

$$\Phi_{1,2} = \alpha_1 \Phi_1 + \alpha_2 \Phi_2, \tag{1}$$

where α_1, α_2 are arbitrary constants, which should meet the following condition:

$$\alpha_1 \,.\, \Delta_{ion,1} + \alpha_2 \,.\, \Delta_{ion,2} = 0, \tag{2}$$

where $\Delta_{ion,1}$ and $\Delta_{ion,2}$ are ionospheric terms on L1 and L2 frequency, respectively.

For example, a popular ion-free combination is obtained using the following constants:

$$\alpha_1 = \frac{f_1^2}{f_1^2 - f_2^2}, \quad \alpha_2 = -\frac{f_2^2}{f_1^2 - f_2^2}. \tag{3}$$

The differencing of the one-way ionosphere-free carrier phase observations between satellites, stations and time epochs generates the ion-free triple-differenced carrier phases. The observation equation of an ionosphere-free triple-differenced measurement between two receivers i and j, two satellites k and l, and over a time interval dt between epochs t_1 and t_2, can be written as:

$$\Phi^{kl}_{ij,ion\text{-}free,dt} = \rho^{kl}_{ij,dt} + T^{kl}_{ij,dt} + \alpha_1 \varepsilon^{kl}_{ij,1,dt} + \alpha_2 \varepsilon^{kl}_{ij,2,dt}, \tag{4}$$

where $\rho^{kl}_{ij,dt}$ is the triple-differenced geometric range; $T^{kl}_{ij,dt}$ is the triple-differenced tropospheric effect; $\varepsilon^{kl}_{ij,1,dt}$, $\varepsilon^{kl}_{ij,2,dt}$ are triple-differenced phase errors on L1 and L2 frequencies, respectively.

It should be noted that virtually all nuisance parameters that affect the single- or double-differenced observable, namely, clock errors, ionospheric effect and ambiguities are eliminated through triple differencing. If the tropospheric effect is modelled and the coordinates of GPS satellites and the tracking stations are provided, the only remaining unknowns in equation (4) are the coordinates of the LEO satellite. On the other hand, the complicated structure of the covariance matrix due to epoch-by-epoch correlation (resulting in a banded matrix in our differencing scheme) is the major disadvantage of the triple differencing. However, a simple and effective solution to this problem is a decorrelation scheme based on the Cholesky factorization of the covariance matrix. This process replaces the inversion procedure with a simple forward substitution in the solution of the system of linear equations. This facilitates

https://doi.org/10.1017/S0373463303002376 Published online by Cambridge University Press

a simple and fast processing algorithm implemented in both GODIVA and P-KOD. The details of the algorithms and their implementation can be found in Grejner-Brzezinska, (1995); Goad et al., (1996); Kwon, (1997); Grejner-Brzezinska et al., (2002b).

Equation (5) provides an explicit representation of the triple-difference carrier phase ionosphere-free observable.

$$\begin{aligned}\Phi^{kl}_{ij,ion\text{-}free,dt} &= \rho^{kl}_{ij,dt} + T^{kl}_{ij,dt} + \alpha_1 \varepsilon^{kl}_{ij,\mathbf{1},dt} + \alpha_2 \varepsilon^{kl}_{ij,\mathbf{2},dt} \\ &= [\rho^{kl}_{ij} + T^{kl}_{ij}]_{t\mathbf{2}} - [\rho^{kl}_{ij} + T^{kl}_{ij}]_{t\mathbf{1}} + [\alpha_1 \varepsilon^{kl}_{ij,\mathbf{1}} + \alpha_2 \varepsilon^{kl}_{ij,\mathbf{2}}]_{t\mathbf{2}} - [\alpha_1 \varepsilon^{kl}_{ij,\mathbf{1}} + \alpha_2 \varepsilon^{kl}_{ij,\mathbf{2}}]_{t\mathbf{1}}. \end{aligned} \quad (5)$$

Since the observations are nonlinear with respect to the unknowns, equation (5) should be linearized to construct the system of equations in the Gauss-Markov model, which can be solved by the least squares method. Among various approaches such as epoch-by-epoch filtering, multi-epoch batch and sequential adjustment, a multi-epoch batch process was selected for this study. That is, the observation equations are accumulated for a certain predefined time interval, and the positions of LEO are solved in one batch processor. Since triple differences contain only the relative information, i.e., the position change between the epochs, a datum constraint must be imposed. One approach is to provide stochastic *a priori* information for all the unknowns and estimate them using the model of adjustment with stochastic constraints. Another option is to provide a fixed datum reference at any epoch (for example, at the initial epoch) and estimate the remaining unknowns. In this study, the second approach was selected to estimate the LEO orbit by fixing the positions of the first epoch in every processing batch. Consequently, the number of unknowns for the k-epoch batch is $3(k-1)$. The adjustment using stochastic *a priori* information at all epochs was also tested; however, the convergence was significantly slower compared to the case of fixing the first epoch as a datum constraint.

It should be mentioned that fixing the first epoch position (available, for example, from the previous arc solution) might introduce a bias into the solution if the coordinates are not sufficiently accurate. Since the initial coordinates affect the solutions at the following epochs through the variance-covariance matrix, the estimates, especially from the first portion of the batch, might be considerably influenced by the bias. In our test, it has been shown that the first $\sim$120 solutions in a 500-epoch batch appear to be affected by the bias in the initial coordinates of $\sim$5 metres. Therefore, using the results from the forward batch filter, the backward filtering, with the last epoch solution fixed, should be performed to eliminate the bias from the initial coordinates. Naturally, the forward and the backward filtering should be iterated until the solution converges.

Some important processing aspects, addressed earlier by Grejner-Brzezinska et al., (2002a and 2002b) and Kwon et al., (2002), are:

- The accuracy of the *a priori* orbits does not have any effect on achieving the convergence in the precise orbit estimation, as long as the cycle slips are detected and removed.
- As far as the *a priori* values for the first epoch coordinates are of reasonable accuracy (1–5 m), just two iterations (forward plus backward) allow achieving the solution convergence.
- Including the signal from low GPS satellites (below 5°) may improve the results.

https://doi.org/10.1017/S0373463303002376 Published online by Cambridge University Press

Table 3. Cycle slips: summary characteristics for 24-hour data sets of June 14–16, 2001.

	June 14, 2001	June 15, 2001	June 16, 2001
Total number of triple difference combinations	220744	216132	42868
Total number of cycle slips	12926	13902	2526
Ratio	5·8%	6·4%	5·9%

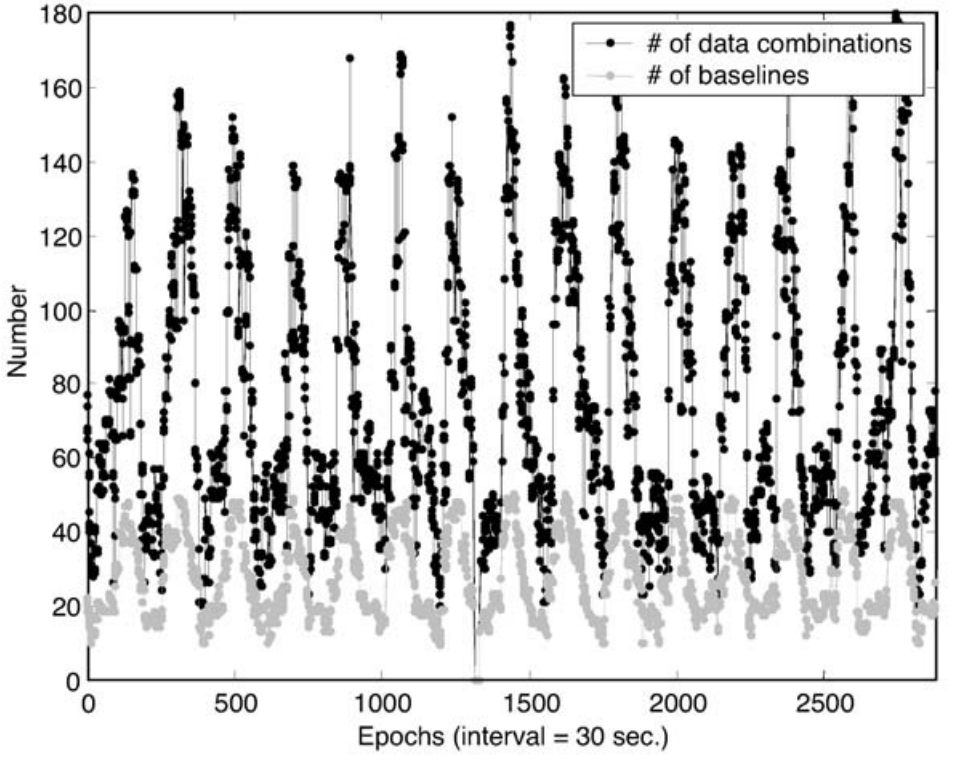


Figure 4. Number of baselines (70 stations used) and triple differences per epoch, June 15, 2001.

- The length of one batch does not have a significant effect on the results, as long as the geometry is uniform.
- If the geometry weakens locally, the best local solution might be obtained for shorter batches, not including the weak geometry parts.

3. TEST DATA. The test data used in the performance analysis were collected on June 14–16, 2001. We analyzed the overall quality of the data in terms of the number of gaps and cycle slips, the effect of the satellite/station geometry and the number of tracking stations, the length of the processing batch and the corresponding positioning quality, as well as the processing speed and efficiency. The maximum number of stations considered was 70, and several configurations of up to 30 stations only were tested. The elevation cut-off routinely used in our processing was 0°

https://doi.org/10.1017/S0373463303002376 Published online by Cambridge University Press

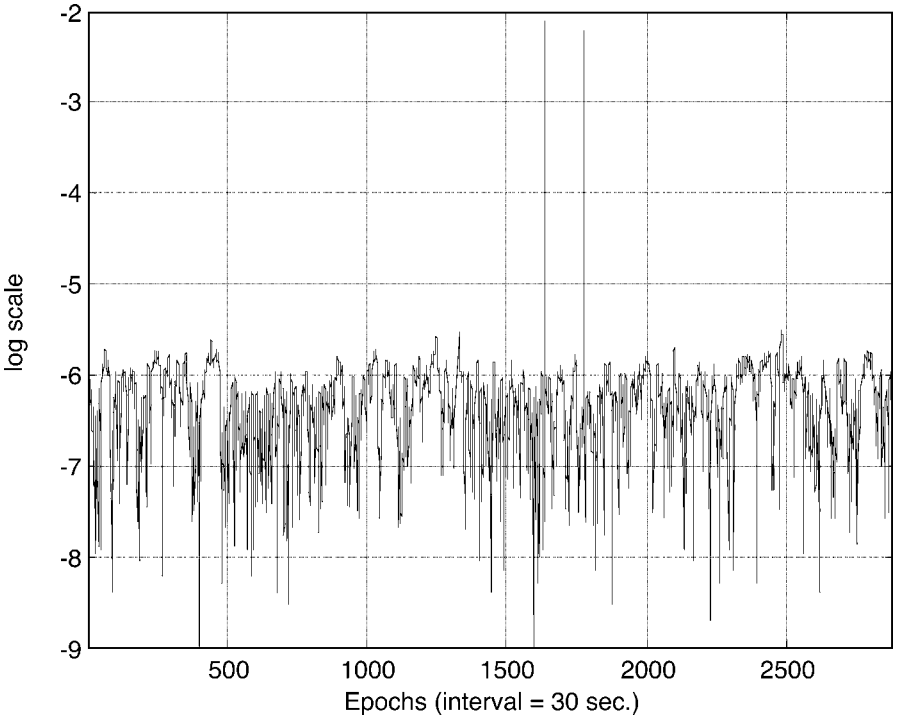


Figure 5. CHAMP estimated clock correction for June 15, 2001, 24-hour data set.

for CHAMP and 10° for the tracking stations. The data spacing was 30 seconds, following the IGS tracking station sampling rate.

The overall quality of the data is presented in Table 3: the average number of CS is about 6 per cent in the daily 24-hour files (~15·3 revolutions), where normally about 3 per cent of all CS happen at the tracking stations, and the remaining about 97 per cent occur at the CHAMP receiver (Bae et al., 2002). Figure 4 illustrates the number of baselines and triple-difference observables for the same data span. The average number of baselines and observations used in the epoch-by-epoch solution ranges from 15–50 and 20–180, respectively. For most of the epochs the Geometric Dilution of Precision (GDOP) is bounded by four with the majority of values below three; however, several local maxima for GDOP can reach six and above, resulting usually in a local singularity. In addition, Figure 5 illustrates the behaviour of the CHAMP clock that, as can be observed in the figure, occasionally displays some unexpectedly large corrections (around epochs 1625 and 1775).

4. PERFORMANCE ANALYSIS.

4.1. *The effect of the number of tracking stations.* Table 4 summarizes the effect of varying the number of tracking stations on the accuracy and efficiency of the CHAMP orbit determination. The number of stations can affect the number of processing batches, while the length of the batch is determined by the data gaps in the CHAMP data, cycle slips, and large GDOP that introduce singularities to the solution. A greater number of stations could mitigate the weak geometry problem,

https://doi.org/10.1017/S0373463303002376 Published online by Cambridge University Press

Table 4. Effect of the number of tracking stations: 24-hour summary characteristics.

Data set	Number of tracking stations	Number of data gaps and their total duration [epochs]	Number of data batches processed	Average fit to the dynamic solution 3D RMS [m]	Processing time (CS detected using the approximated dynamic orbit)
June 14	30	3 (58)	8	0·56	56
	40		9	0·71	50
	50		6	0·62	77
	60		6	0·63	90
	70		7	0·70	94
June 15	30	1 (19)	10	0·55	39
	40		8	0·64	49
	50		7	0·53	59
	60		7	0·53	71
	70		6	0·53	88
June 16	30	2 (32)	14	0·59	49
	40		12	0·56	65
	50		12	0·56	76
	60		12	0·56	95
	70		12	0·57	113

Table 5. Processing time in minutes, forward filter only (cycle slips detected during the data reduction using the approximated dynamic orbit).

	Number of epochs		
	300	400	500
Number of stations			
40	10	11	14
50	12	14	17
60	15	16	20

Table 6. Processing time in minutes, forward and backward filters. Cycle slips detected during the preprocessing using SNR; the numbers in parentheses represent the time used to clean the data (Grejner-Brzezinska et al., 2002a).

	Number of epochs		
	300	400	500
Number of stations			
40	15 (1·57)	19 (1·82)	28 (2·13)
50	18 (1·77)	25 (2·08)	33 (2·45)
60	23 (2·02)	30 (2·38)	39 (2·80)

however, the effect might be local. In general, 40–70 stations provide very similar results, thus increasing the number of tracking stations above 50 might be unnecessary. The overall accuracy of the solution does not seem to be significantly affected by the number of ground stations, except for the cases when singularities combined with weak geometry introduce very short batches that cannot be processed effectively. The

https://doi.org/10.1017/S0373463303002376 Published online by Cambridge University Press

Table 7. RMS fit of the kinematic solution to the dynamic reference orbit (500 epochs).

Component	June 14, 2001 RMS [m]	June 15, 2001 RMS [m]
Radial	0·17	0·12
Along-track	0·19	0·17
Across-track	0·09	0·12
3D RMS	0·27	0·23

Table 8. RMS fit of the kinematic solution to the dynamic reference orbit as function of the number of tracking stations (500 epochs, June 15, 2001).

No. of stations	RMS [m]			
	Radial	Along-track	Across-track	3D
30	0·12	0·17	0·13	0·25
40	0·12	0·16	0·12	0·23
50	0·12	0·16	0·11	0·23
60	0·12	0·16	0·12	0·23
70	0·12	0·17	0·12	0·23

number of ground stations impacts on the processing time, which is an important factor to consider for near real-time applications. The last column in Table 4 shows the processing times on a 1·8 GHz Pentium processor. Furthermore, the estimates of processing time, as a function of the number of tracking stations used, the length of the batch processed and the method of cycle slip detection applied, are provided in Tables 5 and 6. Table 5 refers to the forward solution only while Table 6 presents the processing times for the forward and backward solution. The processing time of a 500-epoch batch (roughly about 2·5 orbits) currently takes less than 20 minutes, indicating that near real-time processing capability is provided. The 3D RMS fit to the dynamic solution listed in Table 4 is relatively high as it covers the entire 24 hours of data and includes the parts of the trajectory affected by a weak geometry. The accuracy of the kinematic orbit can be very high if the geometry is strong and no data gaps exist in the data batch of interest. For example, Table 7 displays a good fit to the reference truth for epochs 1400–1900 for two consecutive days, June 14 and 15 (on June 16 there was a data gap during that time period). In addition, Table 8 illustrates the RMS fit to RSO of the 500-epoch data batch as a function of the number of tracking stations. Clearly, as already indicated, the number of tracking stations does not have a significant effect on the overall solution accuracy if sufficient GPS data are available even for the lowest number of tracking stations.

4.2. *Smoothed orbit*. The solutions analyzed in the previous sections may display local spikes in the residual plot (P-KOD minus RSO), as shown in Figure 6, primarily due to locally weaker geometry and possible undetected CS. In order to achieve a smooth trajectory, an averaging window of 21 epochs (Equation 6) is applied to the kinematic solution.

$$X_i = \frac{X_{i-10} + X_{i-9} + \cdots + X_i + \cdots + X_{i+9} + X_{10}}{\text{Window size}}. \tag{6}$$

https://doi.org/10.1017/S0373463303002376 Published online by Cambridge University Press

Table 9. Smoothed orbits, June 15, 2001, 500 epochs: summary characteristics (corresponds to Table 7).

Component	Mean [m]	RMS [m]
Radial	0·120	0·104
Along-track	−0·006	0·161
Across-track	0·010	0·118
3D		0·225

Table 10. RMS fit to the reference solution of the original kinematic and the smoothed orbits, 500 epochs: summary characteristics (data cleaned using SNR).

Component	Original solution RMS [m]	Smoothed solution RMS [m]
Radial	0·12	0·10
Along-track	0·25	0·21
Across-track	0·19	0·15
3D RMS	0·33	0·28

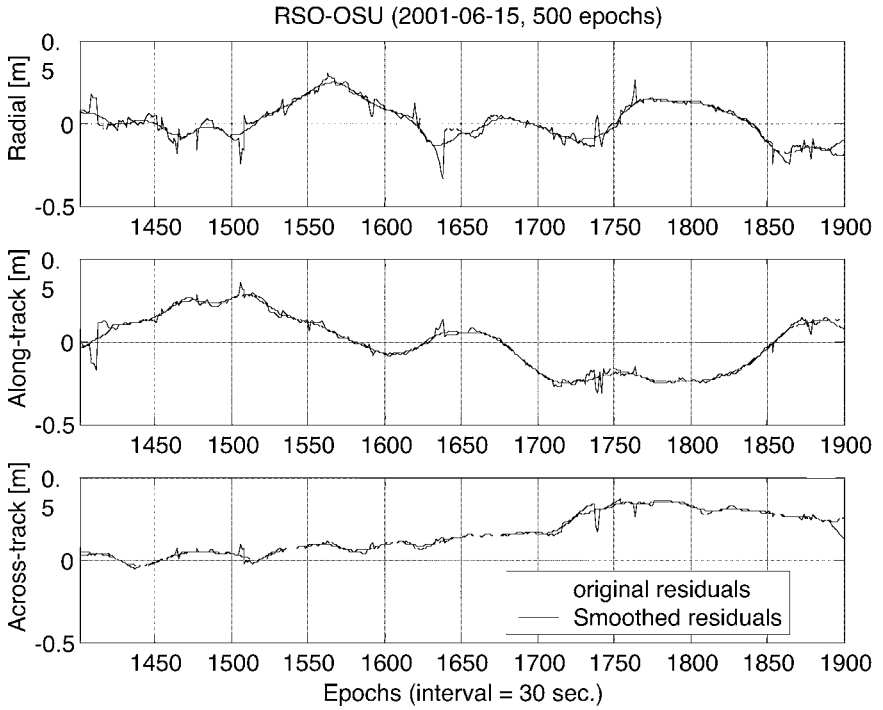


Figure 6. Direct kinematic solution and smoothed orbits, June 15, 2001, 500 epochs.

The effective orbit smoothing, removing the effects of undetected CS is possible due to the fact that any CS affects only one triple difference, and thus, only a local spike occurs in the solution. The comparison of the direct and smoothed orbits is presented in Figure 6 and Table 9. A comparison of Tables 7 and 9 indicates that the smoothing

https://doi.org/10.1017/S0373463303002376 Published online by Cambridge University Press

Table 11. Effect of the processing batch length on the accuracy of the final orbit: RMS fit to RSO.

Arc length	Mean [m]			RMS [m]			
	Radial	Along-track	Across-track	Radial	Along-track	Across-track	3D
300	0·03	0·07	0·06	0·09	0·13	0·04	0·16
400	0·02	0·01	0·10	0·11	0·16	0·09	0·21
500	0·01	−0·01	0·15	0·12	0·17	0·12	0·23

Table 12. The RMS fit to the reference truth per revolution, June 15, 2001.

Revolution (time epochs)	RMS [m]			
	Radial	Along-track	Across-track	3D
1 (1401:1587)	0·11	0·10	0·04	0·16
2 (1588:1744)	0·09	0·11	0·07	0·16
3 (1745:1931)	0·12	0·14	0·12	0·22

Table 13. The number of triple differences and cycle slips per revolution, June 15, 2001.

Revolution (time epochs)	Number of observations	Number of cycle slips	Ratio
1 (1401:1587)	14689	760	5·2%
2 (1588:1744)	14976	771	5·1%
3 (1745:1931)	14621	1055	7·2%

process did not significantly improve the solution in this case. However, in situations where a larger number of spikes were observed, the RMS fit to the reference orbit may improve by $\sim$15 per cent if smoothing is applied, as presented in Table 10.

4.3. *The effect of the processing batch length.* Since the tracking geometry and the number of observations per epoch vary along the trajectory, the length of the processing batch will have an effect on the final accuracy of the trajectory considered. For example, if quality observables under low, uniform GDOP were available for 300 epochs, the resulting orbit accuracy would be high. However, if the accumulation of the normal equations is continued, including weaker geometry, the overall accuracy will drop (even though the effect will be local). Thus the GDOP and the total number of observations per epoch should be tested for the entire data set under consideration and the appropriate batch length should be selected to increase the local fit. An example of the effect of the batch length including varying geometry is presented in Table 11, where the fit to the reference truth is estimated for the batch length of 300, 400 and 500 epochs. Table 12 illustrates a typical RMS fit to a reference dynamic solution for three consecutive orbital revolutions of CHAMP estimated by P-KOD. The last revolution listed in Table 12 displays about a 25 per cent worse fit to the reference truth, mainly due to a smaller number of observations per epoch and a greater number of cycle slips, as shown in Table 13. Again, it is clear that the geometry and the number of observations strongly affect the final quality of the kinematically estimated orbit.

https://doi.org/10.1017/S0373463303002376 Published online by Cambridge University Press

Table 14. Quality of the overlapping orbits: summary of characteristics, June 15, 2001.

	RMS [m]				RMS of fit of the overlapping part [m]			
Data span	Radial	Along-track	Across-track	3D	Radial	Along-track	Across-track	3D
A (1501:1900)	0·12	0·16	0·11	0·23	0·07	0·07	0·01	0·10
B (1501:1900)	0·11	0·12	0·11	0·20				

4.4. *The quality of the overlapping orbits.* One of the measures of orbit quality is the orbit overlap, where two segments of the trajectory, having a common part, are processed independently. Naturally, a better fit of the overlapping segments indicates a better internal consistency of the estimated orbit. As an example, Table 14 displays a summary of the characteristics of the overlapping orbits, each 500 epochs long, with a common 400-epoch segment.

4.5. *Velocity estimation.* The velocities in radial, along and across-track directions were obtained by a numerical differentiation of the kinematic orbit, using Equations 7–9 (for $\Delta t = 30$ s).

$$V(X)_i = \frac{X_{i+1} - X_{i-1}}{2\Delta t}, \tag{7}$$

$$V(Y)_i = \frac{Y_{i+1} - Y_{i-1}}{2\Delta t}, \tag{8}$$

$$V(Z)_i = \frac{Z_{i+1} - Z_{i-1}}{2\Delta t}. \tag{9}$$

A smoothing process, or a low pass filtering could be applied to the velocity estimates to reduce the effects of possible noise amplification due to the numerical differentiation. An example of the velocity fit to the dynamic reference solution (less than 1 mm/s 3D RMS) is presented in Figure 7 and Table 15.

5. SUMMARY AND CONCLUSIONS. A fast and efficient algorithm for geometric determination of LEO trajectories based on triple-differenced carrier phases has been developed and implemented. A major issue in the kinematic approach is LEO data cleaning and cycle slip detection. Due to the low SNR from low GPS satellites and the high dynamics of the CHAMP satellite moving in the middle of the ionospheric layer, detection of outliers and CS is complicated and conventional methods might not suffice. A combination of methods presented here delivers satisfactory results, however, the most efficient CS detection can be presently achieved using an approximated dynamic solution.

The kinematic solution performance was demonstrated using CHAMP orbital data combined with a varying number of tracking station data and their changing geometry. The achievable 3D accuracy of the estimated 500-epoch orbits and velocities are better than 30 cm and 1 mm/s, respectively, with respect to the published dynamic solution for CHAMP. Since the solution is sensitive to the geometry, the number of observations and the data gaps, the local accuracy for shorter batches is much better, and can reach 15 cm in 3D. It is expected that better accuracy might

https://doi.org/10.1017/S0373463303002376 Published online by Cambridge University Press

Table 15. Comparison of the P-KOD velocity estimates with the reference dynamic solution, June 15, 2001, 500 epochs: summary characteristics.

Component	Mean [m/s]	RMS [m/s]
Radial	$-2{\cdot}442 \times 10^{-6}$	$7{\cdot}469 \times 10^{-4}$
Along-track	$1{\cdot}560 \times 10^{-5}$	$4{\cdot}835 \times 10^{-4}$
Across-track	$4{\cdot}660 \times 10^{-6}$	$3{\cdot}602 \times 10^{-4}$
3D		$9{\cdot}598 \times 10^{-4}$

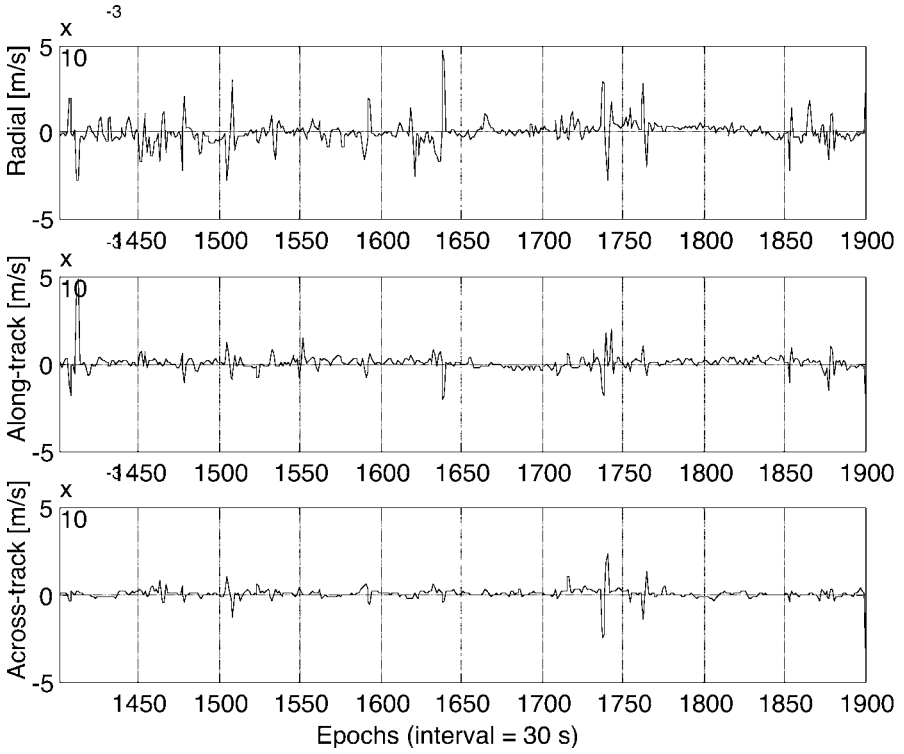


Figure 7. Comparison of the P-KOD velocity estimates with the reference dynamic solution, June 15, 2001, 500 epochs.

be achievable if IGS tropospheric zenith delay data were used instead of standard atmospheric corrections.

The processing times are short, and depend on the number of stations and the number of data batches processed. A 24-hour data set including 60 tracking stations can be processed in less than 1·5 hours. However, for near-real-time applications a single revolution (with the selected side overlaps for better accuracy) should normally be processed; this takes less than 10 minutes. The overall accuracy (except for the occasional locally weak solution) meets the requirements for near-real-time LEO orbit quality to support the occultation events for the atmospheric study (Zhao, 1998).

Despite the high achievable accuracy, the remaining problems are data discontinuities and local singularities caused by the weak geometry and cycle slips,

https://doi.org/10.1017/S0373463303002376 Published online by Cambridge University Press

where no solution or weak solution is available. This can only be corrected by implementing a dynamic force model.

REFERENCES

Bae, T-S., Kwon, J. H. and Grejner-Brzezinska, D. A. (2002). Data Screening and Quality Analysis for Kinematic Orbit Determination of CHAMP Satellite, *Proceedings, ION Technical Meeting, January 28–30, San Diego, California, CD ROM*.

Bisnath, S. B. and Langley R. B. (1999). Precise a posteriori Geometric Tracking of Low Earth Orbiters with GPS, *Canadian Aeronautics and Space Journal*, **45**, 245–252.

Bisnath, S. B. and Langley R. B. (2001a). Precise Orbit Determination of Low Earth Orbiters with GPS Point Positioning, *Proceedings, ION Technical Meeting, January 22–24, Long Beach, CA, CD ROM*.

Bisnath, S. B. and Langley R. B. (2001b). High-Precision Platform Positioning with a Single GPS Receiver, *Proceedings, ION GPS, September 11–14, Salt Lake City, Utah, CD ROM*.

Bock, H., Hugentobler, U. and Beutler, G. (2001). Kinematic Orbit determination for Low Earth Orbiters (LEOs). IAG Scientific Assembly, Budapest, *Vistas for Geodesy in the New Millenium*, Adam J., Schwarz K. P. (Eds), Springer-Verlag Berlin Heidelberg, IAG, **125**, 322–328.

Byun, S. H. (1998). Satellite Orbit Determination Using GPS Carrier Phase in Pure Kinematic Mode, *University of Texas*, *PhD dissertation*.

Byun, S. H. and Schutz, B. E. (2002). Improving satellite orbit solution using double-differenced GPS carrier phase in kinematic mode, *Journal of Geodesy*, **75**, 533–543.

Goad, C. C., Grejner-Brzezinska, D. A. and Yang, M. (1996). Determination of High-Precision GPS Orbits Using Triple Differencing Technique, *Journal of Geodesy*, **70**, 655–662.

Grejner-Brzezinska, D. A. (1995). Analysis of GPS Data Processing Strategies: In Search of Optimized Routine of Orbit and Earth Rotation Parameter Recovery, *Department of Geodetic Science and Surveying, OSU, Departmental Report No. 432*.

Grejner-Brzezinska, D. A., Kwon, J., Bae, T-S. and Hong, C-K. (2002a). Precise Position Determination in Space with GPS, *Proceedings, ION GPS, September 24–27, CD ROM*.

Grejner-Brzezinska, D. A., Kwon, J. H. and Shum, C. K. (2002b). The Ohio State University IGS LEO/GPS Pilot Project: Status and Future Plans, *Navigation*, **49**, 11–19.

Grejner-Brzezinska, D. A., Ge, S., Kwon, J. H., Shum, C. K. and Zhao, C. Y. (2001). GPS/LEO Rapid Orbit Determination in Support of GPS Meteorology: Status and Future Plans, *Vistas for Geodesy in the New Millenium*, IAG Scientific Assembly, Budapest, Hungary, September 2–7, Springer-Verlag Berlin Heidelberg, 316–321.

Koenig, R., Zhu, S. Y., Reigber, Ch., Neumayer, K.-H., Meixner, H., Galas, R., Baustert, G. and Schwintzer, P. (2002). CHAMP Rapid Orbit Determination for GPS Atmospheric Limb Sounding, *Advances in Space Research*, **30**, 289–293.

Kwon, J. (1997). The orbit determination software GODIVA at the Ohio State University, Department of Geodetic Science and Surveying, OSU, Departmental Report No. 438.

Kwon, J. H., Grejner-Brzezinska, D. A. and Hong, C-K. (2002). Kinematic Orbit Determination of Low Earth Orbiter using Triple Differences, *Proceedings, ION Technical Meeting, January 28–30, San Diego, California, CD ROM*.

Reigber, Ch., Luehr, H. and Schwintzer, P. (2002). CHAMP Mission Status, *Advances in Space Research*, **30**, 129–134.

Svehla, D. and Rothacher, M. (2001). Kinematic Orbit Determination of LEOs Based on Zero or Double-difference Algorithms Using Simulated and Real SST GPS Data, IAG Scientific Assembly, Budapest, *Vistas for Geodesy in the New Millenium*, Adam J., Schwarz K. P. (Eds), Springer-Verlag Berlin Heidelberg, IAG, **125**, 322–328.

Svehla, D. and Rothacher, M. (2002). Kinematic and Reduced-Dynamic Precise Orbit Determination of Low Earth Orbiters, presented at EGS, Nice, France, submitted to *Advances in Geosciences*, 2002.

Yang, M. (1995). New GPS Measurement Modeling Technique for Orbit Determination and Precise Kinematic Positioning, *Department of Geodetic Science and Surveying, OSU*, *Departmental Report No. 431*.

Zhao, C. Y. (1998). The sensitivity of atmospheric temperature retrieved from radio occultation technique to orbit errors of GPS and LEO satellite, *GeoForschungsZentrum Potsdam, Scientific Technical Report STR98/23*.

https://doi.org/10.1017/S0373463303002376 Published online by Cambridge University Press